PROCEEDINGS OF SPIE

SPIEDigitalLibrary.org/conference-proceedings-of-spie

Mid-infrared spectroscopy with a fiber-coupled tuneable quantum cascade laser for glucose sensing

Jernelv, Ine, Strøm, Karina, Hjelme, Dag Roar, Aksnes, Astrid

Ine L. Jernelv, Karina Strøm, Dag Roar Hjelme, Astrid Aksnes, "Mid-infrared spectroscopy with a fiber-coupled tuneable quantum cascade laser for glucose sensing," Proc. SPIE 11233, Optical Fibers and Sensors for Medical Diagnostics and Treatment Applications XX, 1123311 (20 February 2020); doi: 10.1117/12.2543984

SPIE.

Event: SPIE BiOS, 2020, San Francisco, California, United States

Mid-infrared spectroscopy with a fiber-coupled tuneable quantum cascade laser for glucose sensing

Ine L. Jernelv*, Karina Strøm, Dag Roar Hjelme, and Astrid Aksnes

Department of Electronic Systems, Norwegian University of Science and Technology (NTNU), O.S. Bragstads plass 2A, 7491 Trondheim, Norway

ABSTRACT

A fiber-coupled transmission spectroscopy setup using a pulsed external-cavity quantum cascade laser (EC-QCL, 1200-900 cm^{-1}) has been developed and demonstrated for measurements of aqueous solutions. The system has been characterised with regard to the laser noise and optimal optical pathlength. Solutions with glucose were used to further test the setup, and glucose concentrations down to physiologically relevant levels (0-600 mg/dL) were investigated. Albumin, lactate, urea, and fructose in various concentrations were added as interfering substances as their absorption bands overlap with those of glucose, and because they may be of interest in a clinical setting. Analyte concentrations were predicted using partial least-squares (PLS) regression, and the root-mean-square error of cross-validation for glucose was 10.7 mg/dL. The advantages of using a convolutional neural network (CNN) for regression analysis in comparison to the PLS regression were also shown. The application of a CNN gave an improved prediction error (8.3 mg/dL), and was used to identify important spectral regions. These results are comparable to state-of-the-art enzymatic glucose sensors, and are encouraging for further research on optics-based glucose sensors.

Keywords: Quantum cascade laser, mid-infrared spectroscopy, biomedical sensing, laser spectroscopy, glucose

1. INTRODUCTION

The research effort on biomedical sensors is growing and rapidly developing, with blood glucose monitoring dominating the market for biomedical sensors.[1] Glucose sensors are vital for diabetic patients, as these patients have to monitor their blood glucose level in order to prevent long- and short-term complications. Most commercial glucose sensors today base their measurements on enzymatic reactions, and can be used either for finger-prick tests, or for minimally invasive continuous glucose monitoring (CGM). These sensors suffer a loss of accuracy and reliability over time due to sensor and enzyme degradation, and must typically be changed every 1-2 weeks. Optical spectroscopy may be a better alternative for CGM, as it is reagent-free and non-destructive.

Several research groups have worked with systems for biomedical laser spectroscopy in the mid-infrared following the commerical availability of EC-QCLs. These systems have mainly used either free-space configurations with liquid samples in transmission cells,[2,3] or fiber-coupled setups with either transmission, reflectance, or attenuated total reflection (ATR) sensing modalities.[4–7] Fiber-coupled setups are more practical for portable sensor development, while free-space setups can potentially be used for larger systems in e.g. intensive care. However, there have been few detailed studies using EC-QCLs as sources in fiber-coupled configurations.

In this study we present a fiber-coupled spectroscopy setup aimed at continuous glucose monitoring, with a broadly tuneable EC-QCL as a source. The system noise as a function of pathlength is characterised. The performance of the system is tested using aqueous solutions with glucose and several analytes with overlapping absorption bands. We also show an application of a convolutional neural network as a method for regression analysis, and compare its performance to standard partial least-squares regression.

* ine.jernelv@ntnu.no; phone +47 73594400

Optical Fibers and Sensors for Medical Diagnostics and Treatment Applications XX, edited by Israel Gannot
Proc. of SPIE Vol. 11233, 1123311 · © 2020 SPIE · CCC code: 1605-7422/20/$21 · doi: 10.1117/12.2543984

2. METHODS

2.1 Experimental setup

The experimental setup (see Fig. 1) in this study consisted of a mid-infrared laser with a controller, a photodetector, an analog-to-digital converter card (ADC), a control computer, and a transmission sensing interface between two optical fibers. A pulsed external-cavity quantum cascade laser (EC-QCL, Hedgehog-UT, Daylight Solutions Inc., USA) was used as the light source. The laser was tuneable in the range 1200-900 cm^{-1} (8.33-11.1 µm), and was operated with a pulse length of 500 ns and a repetition rate of 100 kHz, for a 5% duty cycle. This wavelength range covers the main vibrational bands of glucose in the mid-infrared fingerprint region. An MCT detector (PCI-4TE, Vigo System S.A., Poland) with a 2x2 mm detector element was used to detect the infrared signal. This detector had a 4-stage thermoelectric cooling system, and operated at -75.2°C with a detectivity of 3×10^9 $cmHz^{1/2}W^{-1}$ at 10.6 µm. The laser beam was focussed into a fiber with an optical assembly mounted on the laser (OKSI Fibers Inc., USA). Silver halide fibers (Art photonics GmbH, Germany) were used to guide the light and sensing was done in a 200 µm gap between two fibers. The in-coupling fiber had a core diameter of 400 µm, while the out-coupling fiber had a core diameter of 600 µm.

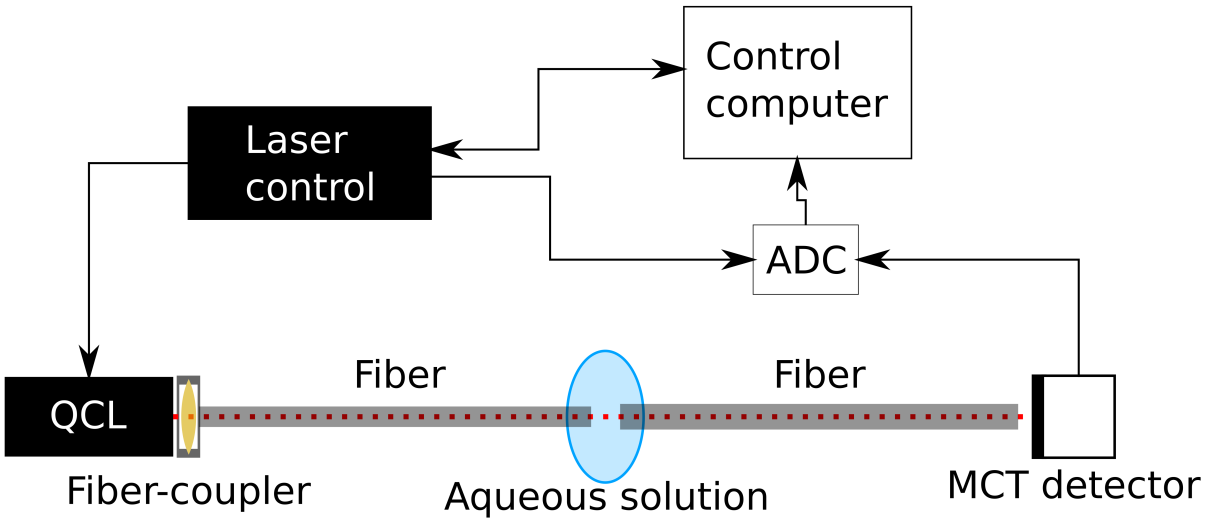

Figure 1: Sketch of the transmission setup. The arrows indicate the direction of data or information transfer.

2.2 Data recording

The analog signal from the MCT detector was recorded and digitised by an M2p.5946-x4 analog-to-digital converter card (Spectrum-Instrumentation GmbH, Germany). This board could digitise the signal at 80 MS/s with 16 bit resolution. The laser controller had a DB-15 connector with 15 pins for I/O signals. One of these pins generated a rising edge TTL at the start of each laser scan. This signal was used to trigger data acquisition. A scan speed of 275 cm^{-1}/s was used, and data recording was active for 1 second after the trigger. Spectra were recorded in the wavenumber range 1200-925 cm^{-1}.

Spectra were produced from the detected signal by integrating each laser pulse, and then creating data points by averaging n pulses, with $n = 255$ for these measurements. Additionally, for each measurement 10 laser scans were averaged to produce a raw spectrum, for a total measurement time of 10 s. This averaging was found to yield low measurement noise in a previous study.[7] Final measurement spectra were then made by subtracting a background spectrum of demineralised water.

2.3 Sample preparation

25 samples were prepared containing glucose, albumin, lactate, urea, and fructose, see Table 1 for an overview of analyte concentrations. Analyte concentrations in the samples were randomised according to an optimal design

model, in order to maintain experimental robustness with relatively few samples. A quadratic Scheffe model with A-optimality design was used for this sample set.

Analytes were dissolved in a phosphate-buffered saline (PBS) solution, which was made from PBS tablets and demineralised water. PBS is a solution with ion concentrations similar to the concentrations in the human body, and works as a buffer to maintain a constant pH. A separate set of seven samples with only glucose in demineralised water was prepared, with a concentration range of 0-500 mg/dL.

Table 1: Concentration ranges for analytes in the complex aqueous solutions.

Analyte	Concentration range
Glucose	0-600 mg/dL
Albumin	0-40 g/L
Lactate	0-250 mg/dL
Urea	0-250 mg/dL
Fructose	0-250 mg/dL

The additional analytes in the complex solutions were included based on their physiological relevance, as they are present in blood plasma and interstitial fluid in humans. The concentrations of lactate, urea, and fructose are exaggerated compared to physiological concentrations in order to increase the interference with the glucose levels.

2.4 Data analysis

All data analysis in this study was done with the freely available software SpecAnalysis, which is available on Github (https://github.com/jernelv/SpecAnalysis). This software is written in the Python programming language, and provides a system for pre-processing, feature selection, and multivariate analysis of spectral data.

2.4.1 Standard regression analysis

The absorbance spectra acquired from the different solutions were first analysed with partial least-squares (PLS) regression. All samples were measured five times over a period of two weeks, giving five separate datasets. Analyte prediction was evaluated with root-mean-square error of cross-validation (RMSECV), and additionally with the coefficient of determination (R^2), as RMSE-values are scale-dependent. Cross-validation (CV) was done with either leave-one-out (LOOCV) within datasets, or leave-one-dataset-out (LDOCV) between datasets.

The samples containing only glucose were analysed with PLS regression using 1 latent variable. PLS regression with 6 latent variables was used for the complex solutions. The data was mean centered and scaled prior to the regression analysis, and no other pre-processing was used.

2.4.2 Convolutional neural network

For further investigation of the acquired spectra we used a convolutional neural network (CNN) for concentration prediction. CNNs are a type of data mining model commonly used for e.g. image analysis, and have recently been applied to one-dimensional vibrational spectra.[8] CNNs are a variant of artificial neural networks (ANNs), which have previously been used for e.g. concentration prediction of glucose data from FTIR spectroscopy.[9] These ANNs used fully connected layers instead of convolutional layers, and had issues with overfitting on spectral data.

Neural networks are based on connected artificial neurons, where each neuron has an activation function that transforms an input into an output. These neurons are arranged in layers (see Fig. 2), which can be divided into input, output, and hidden layers. In standard ANNs the output of a neuron is used as input in every neuron in the next layer, giving fully connected layers. In a CNN the input is convolved using one or more kernel functions, which effectively reduces the number of times the output is used as an input in the next layer. This gives fewer connections and hidden variables in total, and CNNs are therefore computationally faster and are less prone to overfitting than equivalent fully-connected models. Neurons are connected together with weighted connections, which are set to a random initial value. The weights are then adjusted during the training phase.

For this study, we used a CNN with 2 hidden layers, and other CNN parameters were varied in order to find the optimal model. We searched through different ranges of layer size (5-35), kernel size (5-35), dropout rate (0-0.2) and stride (1-5). The stride is the step size of the kernel, while the dropout rate indicates the amount of randomly dropped neurons in the model, which is a method used to prevent overfitting.

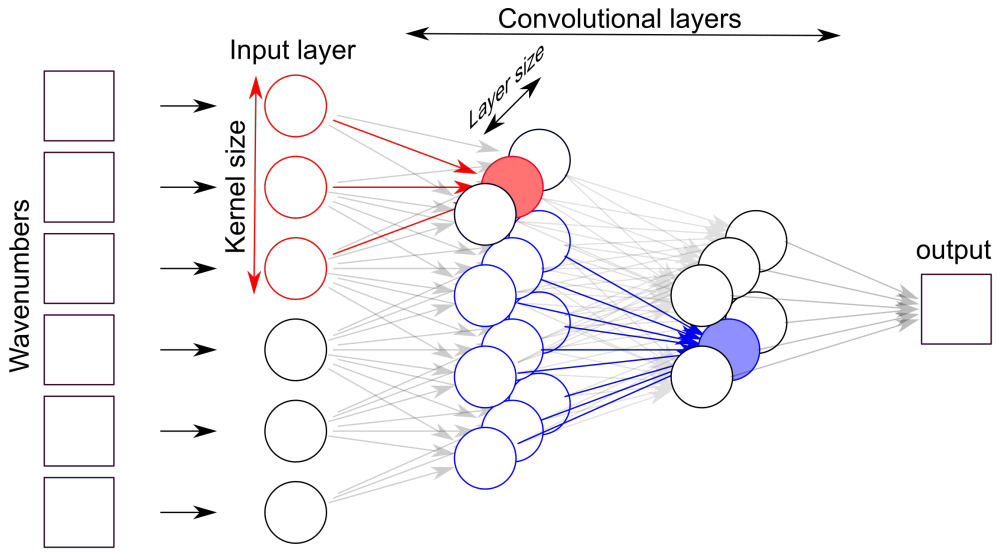

Figure 2: Example of a CNN with two convolutional (hidden) layers, where kernel and layer sizes are indicated. Each circle represents a neuron. A few neurons and connections have been highlighted in order to show the flow of input and output to and from neurons.

Neural networks are often seen as "black boxes" where the relation between the input data and the output regression is treated as an unknown. However, it is possible to look into this black box by operating directly on the output from neurons. The output of a neuron in a CNN is a product of a kernel used on a specific region of the spectrum. A feature selection method applied on these outputs can therefore be used to find regions of interest. In order to do this, we implemented a method for stability feature selection (SFS).[10] SFS is done by randomly selecting subsets of the data, and then retraining the last layer of the CNN. Features can then be scored according to the change in weights.

3. RESULTS AND DISCUSSION

3.1 Pathlength

Pathlength is an important parameter for transmission spectroscopy, as a trade-off between signal strength and noise level. For mid-infrared spectroscopy of aqueous media, such as in biomedical spectroscopy, pathlength is particularly significant because of the strong water absorption. Transmission FTIR spectroscopy has been limited to a few tens of micrometers, as FTIR sources have low spectral power density. A longer optimal pathlength can be expected for QCL systems, as they have several orders of magnitude higher spectral power density. Brandstetter et al.[2] demonstrated that a pathlength of approximately 140 µm was optimal for their QCL transmission setup, which was longer than the theoretical optimum.

System noise as a function of pathlength was investigated by recording transmission spectra through demineralised water with pathlengths in the range 130-260 µm. Full spectra were acquired at each position, as well as 100 000 pulses at 1190.5 cm^{-1} (8.4 µm). The relative standard deviation (RSD) when averaging over 255 pulses from the single-wavelength measurements is shown in Fig. 3a. The RSD is relatively constant at approximately 0.07% at shorter pathlengths, and then rapidly increases for pathlengths >210 µm. Figure 3b shows the measured intensities of single laser scans at different pathlengths. The shape of these spectra is a convolution of the laser emission profile and the water absorption.

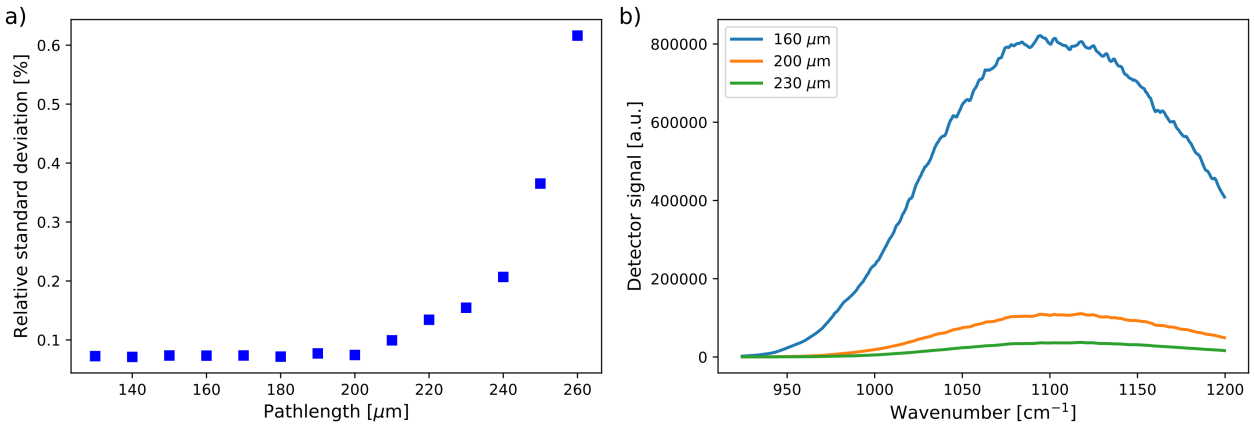

Figure 3: a) Relative standard deviation of laser pulse intensity at 8.4 µm for different transmission pathlengths. b) Signal intensity of single laser scans for different pathlengths. In both cases measurements were done with demineralised water between the fibers.

These results indicate that the laser noise dominates up to a pathlength of 210 µm. At longer pathlengths, the signal strength through the water decreases, until a point where detector noise becomes a significant part of the system noise. On the other hand, the absorbance signal from analytes increases linearly with an increase in pathlength. One should therefore use long pathlengths, as long as the system noise is not increased.

This was further validated by calculating the signal-to-noise ratio (SNR) as a function of pathlength based on full measurements. Standard samples of 100 mg/dL glucose in demineralised water were used for these measurements. We then used the same procedure as Brandstetter et al[2] to estimate SNR. The absorbance signal from the glucose peak at approximately 1080 cm^{-1} was used as the signal, while the RMS noise in the range 1040-1120 cm^{-1} was used as noise. The resulting plot of SNR as a function of pathlength is shown in Fig. 4c, and a pathlength of 200 µm was used for all further measurements.

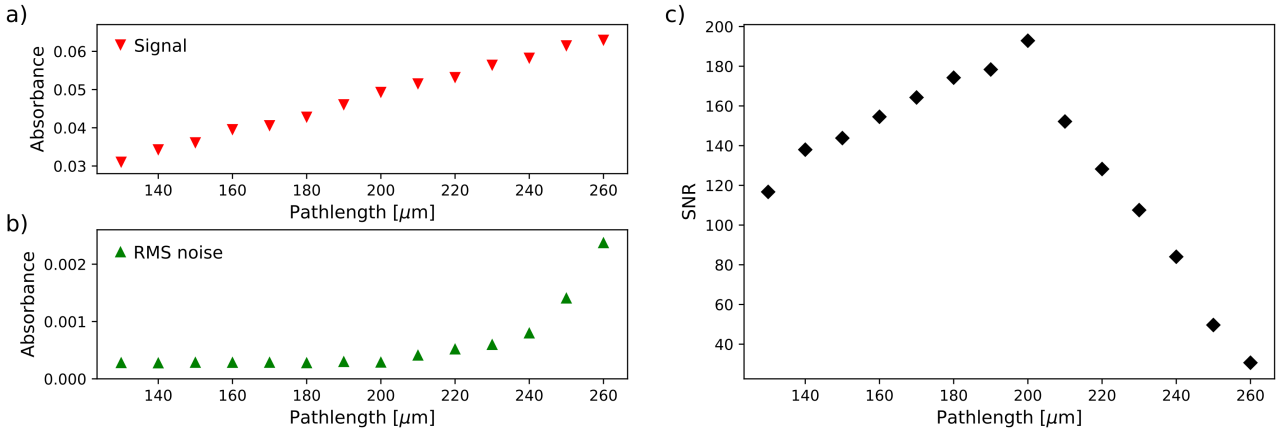

Figure 4: a) Absorbance signal as a function of pathlength, b) RMS noise as a function of pathlength, and c) SNR at 1080 cm^{-1} for a standard 100 mg/dL glucose solution in demineralised water.

With the sensing configuration in this setup, it was anticipated that some light could be lost in the gap between the two fibers, as light diverges when exiting a fiber. A fiber with a larger core was therefore used for the output in order to mitigate this effect. Based on the NA of the fiber (0.3), it was then expected that the output fiber would capture the entire beam. This was also indicated in the absorbance measurements, as the measured signal followed a linear trend as a function of pathlength (see Fig. 4a).

3.2 Glucose spectra

A preliminary characterisation of glucose absorbance spectra was done by measuring different glucose concentrations in water. Absorbance spectra are shown in Fig.5a, with the reference spectrum subtracted. Wavenumbers in the range 969-925 cm^{-1} were not included in the plot, as no absorption features were present.

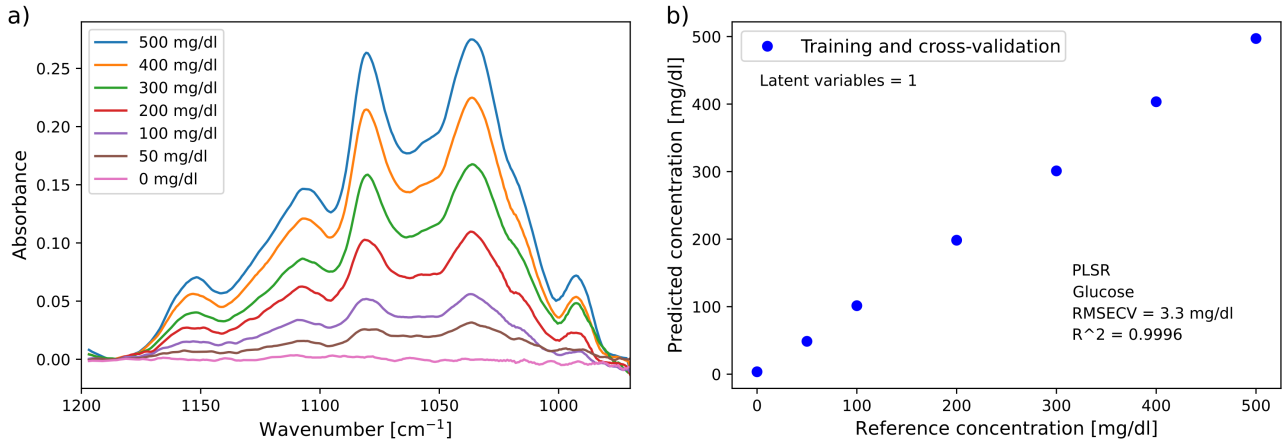

Figure 5: a) Absorbance spectra of aqueous glucose solutions with different glucose concentrations, and b) prediction of glucose concentrations in pure glucose solutions.

A prediction plot with leave-one-out cross-validation (LOOCV) of the pure glucose solutions is shown in Fig. 5b. This analysis was done using PLS regression with one latent variable, and gave an RMSECV of 3.3 mg/dL. For leave-one-dataset-out cross-validation the total RMSECV increased slightly to 4.3 mg/dL, with a coefficient of determination of R^2=0.9994.

3.3 Concentration measurements

For clinical applications, it is necessary to investigate if glucose concentrations can be predicted in the presence of other analytes with interfering absorption bands. Albumin, lactate, urea, and fructose were therefore added to a set of glucose solutions. These analytes were dissolved together with glucose in PBS solutions, to a total of 25 samples. Spectra of the individual analytes are shown in Fig. 6a. All the additional analytes have absorption bands that overlap with those from glucose. PBS also has two absorption bands in this wavelength range, and is scaled down to 1/3 for improved readability. As PBS has the same concentration in all samples it acts as a constant interference in the spectra.

Figure 6b shows a prediction plot for glucose in the complex solutions, with one case of leave-one-dataset-out cross-validation (LDOCV). The total RMSECV for LDOCV was 10.7 mg/dL. The RMSECV for leave-one-out cross-validation (LOOCV) within datasets was 9.4 mg/dL. The other analytes followed the same trend, with somewhat lower prediction errors for LOOCV than for LDOCV. This is as expected, since LOOCV does not capture e.g. between-day variations in the data. The prediction errors for all analytes are summarised in Table 2, and for conciseness only LDOCV is reported.

Table 2: Prediction errors with PLS regression for leave-one-dataset-out cross-validation (LDOCV) of all analytes used in the complex samples.

Analyte	RMSECV	R^2
Glucose	10.7 mg/dL	0.9972
Albumin	1.03 g/L	0.9922
Lactate	7.8 mg/dL	0.9917
Urea	11 mg/dL	0.9874
Fructose	8.7 mg/dL	0.9916

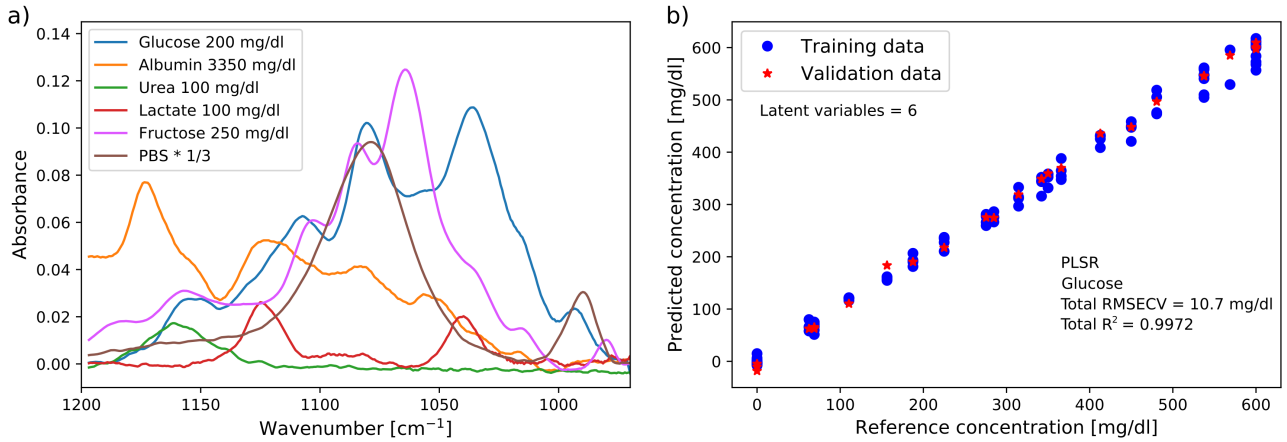

Figure 6: a) Absorbance spectra of different analytes and PBS dissolved in demineralised water with the background spectrum subtracted, and b) prediction of glucose concentrations in the complex solutions with PLSR and leave-one-dataset-out cross-validation, showing one case of the cross-validation.

This performance is comparable to the standard enzymatic glucose sensors used by diabetic patients, and has been found for solutions with analytes that are physiologically relevant for humans. The concentrations used here for lactate, urea, and fructose are higher than what is normally found in e.g. blood plasma or interstitial fluid, and the measurement error achieved for glucose should therefore be sufficient also for in vivo fluids. Measuring with a broadly tuneable laser also allows for simultaneous determination of other analytes which may have clinical significance.

3.4 Prediction with convolutional neural network

For the CNN, the total RMSECV for leave-one-dataset-out cross-validation was 8.3 mg/dL (see Fig. 7a), and for LOOCV the RMSECV was 8.1 mg/dL. Prediction results for all analytes are summarised in Table 3.

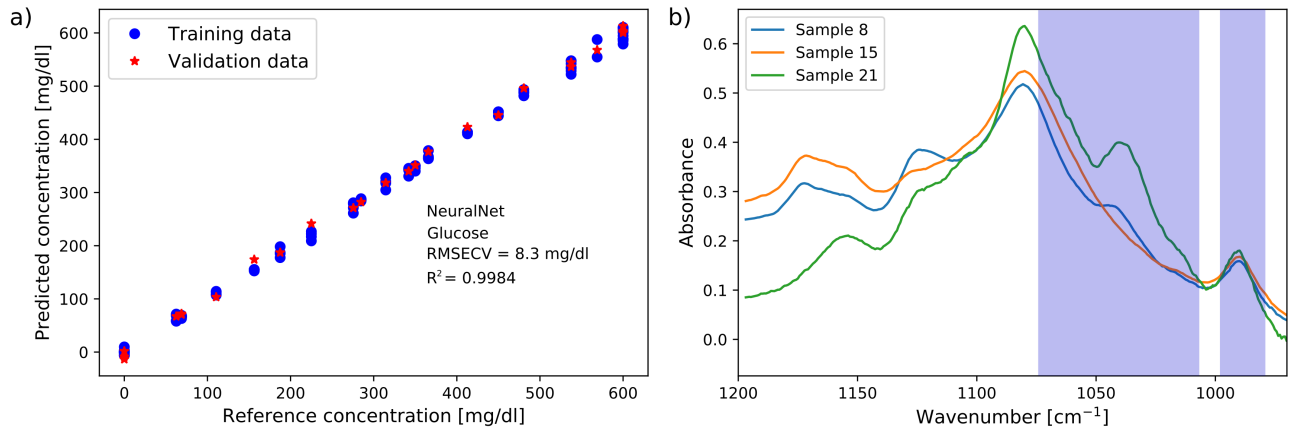

Figure 7: a) Prediction of glucose concentrations with CNN using leave-one-dataset-out cross-validation, showing one case of the cross-validation. b) Example spectra from the complex solutions, where important regions found with CNN and feature extraction have been marked. Glucose concentrations were 63 mg/dL, 0 mg/dL, and 422 mg/dL for Sample 8, 15, and 21 respectively. The other analytes were present in various concentrations.

Prediction errors were consistently lower for all analytes when using CNN as compared to PLS regression. The improvement was largest for glucose and albumin (approx. 20%). The difference was marginal for lactate and urea, which could be related to the lower intensity of their absorption features.

Table 3: Prediction errors with CNN regression for leave-one-dataset-out cross-validation of all analytes used in the complex samples.

Analyte	RMSECV	R^2
Glucose	8.3 mg/dL	0.9984
Albumin	0.89 g/L	0.9946
Lactate	7.5 mg/dL	0.9923
Urea	10.5 mg/dL	0.9885
Fructose	7.2 mg/dL	0.9945

Figure 7b shows the important spectral regions for glucose prediction as determined by CNN and stability feature selection. The important regions are overlayed on three example spectra from the complex solutions. This feature extraction has identified regions that overlap with glucose absorption features, which is not unexpected. It has also marked regions with relatively little interference from other analytes, which can be seen from Fig. 6. This indicates that feature extraction can be used as a tool to find out where the CNN is most sensitive to an analyte of interest. This can be used to e.g. narrow down the region of interest for further sensor development.

4. CONCLUSIONS

Glucose concentrations were predicted with high accuracy in solutions with other analytes with interfering absorption bands. An RMSECV of 10.7 mg/dL was shown with PLS regression, and this was further improved to 8.3 mg/dL with regression based on CNN. Several analytes found in e.g. interstitial fluid were used in these complex solutions, and the low prediction error achieved indicates that accurate in vivo measurements should be possible. Simultaneous determination of several analytes was also demonstrated. This is promising for future development of miniaturised sensors using optical fibers in the mid-infrared.

The high accuracy was in part achieved after a thorough analysis of the system noise. We showed that a pathlength of 200 µm in aqueous solutions could be used without detriment to the noise level. At the same time, this pathlength gave a higher absorbance signal, which resulted in a higher SNR as compared to longer or shorter pathlengths.

We also used a neural network in order to predict glucose concentration, and achieved better prediction errors than those in the PLS regression. The CNN results demonstrate that improved data modelling can be an important tool to achieve better prediction accuracies. Additional information could also be extracted from the CNN, such as the spectral regions where the model was most sensitive.

ACKNOWLEDGMENTS

This work was supported by the Research Council of Norway through the Double Intraperitoneal Artificial Pancreas project, grant number 248872. The project is part of Center for Digital Life Norway and is also supported by the Research Council of Norway's grant 248810.

REFERENCES

[1] Turner, A. P. F., "Biosensors - Sense and sensibility," *Chem. Soc. Rev.* **42**(8), 3184–3196 (2013).

[2] Brandstetter, M., Volgger, L., Genner, A., Jungbauer, C., and Lendl, B., "Direct determination of glucose, lactate and triglycerides in blood serum by a tunable quantum cascade laser-based mid-IR sensor," *Applied Physics B* **110**(2), 233–239 (2013).

[3] Vahlsing, T., Delbeck, S., Budde, J., Ihrig, D., Leonhardt, S., and Michael Heise, H., "Reliable glucose monitoring by ex-vivo blood microdialysis and infrared spectrometry for patients in critical care," *Optical Diagnostics and Sensing XVII: Toward Point-of-Care Diagnostics, Proc. SPIE* **10072** (2017).

[4] Isensee, K., Müller, N., Pucci, A., and Petrich, W., "Towards a quantum cascade laser-based implant for the continuous monitoring of glucose," *The Analyst* **143**(24) (2018).

[5] Liakat, S., Bors, K. a., Huang, T.-Y., Michel, A. P. M., Zanghi, E., and Gmachl, C. F., "In vitro measurements of physiological glucose concentrations in biological fluids using mid-infrared light.," *Biomedical Optics Express* **4**(7), 1083–90 (2013).

[6] Kasahara, R., Kino, S., Soyama, S., and Matsuura, Y., "Noninvasive glucose monitoring using mid-infrared absorption spectroscopy based on a few wavenumbers," *Biomedical Optics Express* **9**(1), 289–302 (2018).

[7] Jernelv, I. L., Strøm, K., Hjelme, D. R., and Aksnes, A., "Infrared spectroscopy with a fiber-coupled quantum cascade laser for attenuated total reflection measurements towards biomedical applications," *Sensors* **19**(23) (2019).

[8] Yang, J., Xu, J., Zhang, X., Wu, C., Lin, T., and Ying, Y., "Deep learning for vibrational spectral analysis: Recent progress and a practical guide," *Analytica Chimica Acta* **1081**, 6–17 (2019).

[9] Bhandare, P., Mendelson, Y., Peura, R. A., Janatsch, G., Kruse-Jarres, J. D., Marbach, R., and Heise, H. M., "Multivariate Determination of Glucose in Whole Blood Using Partial Least-Squares and Artificial Neural Networks Based on Mid-Infrared Spectroscopy," *Applied Spectroscopy* **47**(8), 1214–1221 (1993).

[10] Meinshausen, N. and Bühlmann, P., "Stability selection," *Journal of the Royal Statistical Society. Series B: Statistical Methodology* **72**(4), 417–473 (2010).